Fractal Holey Metal Microlenses with Significantly Suppressed Side Lobes and High-Order Diffractions in Focusing

Yan Jun Liu, Hong Liu, Eunice Sok Ping Leong, Chan Choy Chum, and Jing Hua Teng**

A fractal holey metal microlens based on finite areas of two-dimensional arrays of circular nanoholes is reported. Both experimental and simulation results confirm that the fractal holey metal microlens can significantly suppress both the side lobes and high-order diffractions. The ultra-thin, planar, and compact design of the fractal holey metal microlenses with excellent focusing performance will benefit many applications such as bioimaging, optical trapping, and integrated optics.

1. Introduction

Diffractive focusing elements play an important role in a wide range of applications, including light collimation,[1] beam shaping,[2] and optical manipulation.[3] Among them, Fresnel zone plates (FZPs) are widely used for convenient integration and deployment in various optical systems due to their design flexibility and planar optics in nature.[4] However, most zone plate-based lenses create a halo with substantial intensity (also known as the side lobes), which limits the resolving power and imaging quality of the lenses. It has been shown that photon sieve[5] can greatly suppress the halo effect and achieve high resolution for focusing and imaging. It is similar to a FZP, except that the clear zones in a FZP are replaced by a saturation of non-overlapping holes of set sizes in a photon sieve. Both theoretical and experimental works have been conducted on studying the fundamental properties of photon sieves[6,7] and demonstrating their practical applications.[8–11] Other issues associated with the FZPs are their short focal depth and high chromatic aberration. Fractal zone plates (FraZPs) have therefore been conceptualized and developed to improve the imaging capabilities. A fractal is a geometrical shape whose parts resemble, at least statistically, the whole.[12] Experimental results show that FraZPs can not only increase the focal depth but also reduce the chromatic aberration due to their fractal structures.[13,14]

Future development of nanophotonic integration essentially requires the miniaturization of the focusing elements. The focusing and imaging capabilities of dielectric-based microlenses, either refraction-based or the aforementioned zone plate-based, however, deteriorates greatly as their physical dimensions are further reduced toward a single-/subwavelength scale. Surface plasmons, collective charge oscillations on a metal–dielectric interface, provide opportunities to reduce the size of optical elements by strong confinement of electromagnetic waves.[15–17] Optical components composed of plasmonic materials exhibit enhanced optical transmission,[18–20] nanoscale waveguiding,[21–23] and light generation in subwavelength volumes.[24–26] The principles of diffraction from nanostructured surfaces have been used to control the coupling of light into and out of surface plasmon modes[15] and design plasmonic lenses with subwavelength features as well. Thus far, plasmonic lenses require their subwavelength features be fabricated with variations in size such that each aperture transmits light with a different phase delay.[27–32] However, all the above mentioned plasmonic lenses have been fabricated based on very thick metal films (>100 nm), hence having significantly low efficiency due to the high absorption loss of the metals. For zone plate based plasmonic lenses, we note that they have the same issues as dielectric-based FZPs, especially for the halo effect.[33] Therefore, it is highly desirable to have a plasmonic lens with a versatile design to eliminate these problems.

Herein, we report a fractal holey metal microlens based on finite-areas of two-dimensional arrays of circular nanoholes by combining the concepts of Fractals and photon sieves. We will show that the proposed fractal holey metal microlens can solve the problems to a large extent faced by most plasmonic focusing elements, i.e., the low efficiency, the halo effect, and high-order diffractions. The excellent focusing performance enables our fractal holey metal microlenses promising for many applications in bio-imaging, optical trapping, and integrated optics.

Y. J. Liu, H. Liu, E. S. P. Leong,
C. C. Chum, J. H. Teng
Institute of Materials Research and Engineering
Agency for Science
Technology and Research (A*STAR), 3 Research Link
Singapore 117602, Singapore
E-mail: liuy@imre.a-star.edu.sg; jh-teng@imre.a-star.edu.sg

DOI: 10.1002/adom.201300447

2. Results and Discussion

The generation of the fractal structure was based on the construction of a typical polyadic Cantor fractal set with a specific lacunarity, which can be found elsewhere in more details.[13] In brief, the first step was to define an initiator (stage $S = 0$). Next, at stage $S = 1$, the generator of the set was constructed

by N non-overlapping copies of the initiator, each scaled by a factor $\gamma < 1$. At the following stages ($S = 2, 3, \ldots$), the generation process was repeated for each segment in the previous stage. Once we get the one-dimensional Cantor fractal, which is mathematically described by a binary function $q(\varsigma)$ defined in the interval [0, 1], lacunar FraZPs can be generated by performing a change of coordinates $\varsigma = (r/a)^2$ and rotating the transformed one-dimensional (1D) function around one of its extremes. The resulted FraZPs have a radial coordinate r and an outermost ring of radius a. In general, one has to use four parameters to characterize the fractal holey metal microlens: fractal order, S, scaled factor, γ, the number of residual bars, N, and the lacunarity, ε. We followed the same designs in a previous report[34] and generated a set of FraZPs with varying γ and ε at fixed S and N (see Figure S1a–1d). Among these four designs, the design with $S = 2$, $N = 4$, $\gamma = 1/7$, and $\varepsilon = 1/7$ gives the highest intensity of the main lobe.[34] Therefore, we chose this structure for a further sieve concept design. To generate our fractal holey-metal microlens, we simply replace the transparent zones with isolated, randomly distributed circular holes on a metal film. It is worth mentioning that when we replaced the zones with nanoholes, we adopted the results reported in Ref. [5] where it has been shown that for a photon sieve constructed from a Fresnel zone plate structure, the diameter d of the holes in each ring of width w has an optimum value for the effective contribution to the focus. As discussed in the literature,[5] the hole size and position play an important role on the focusing performance since the light passing through the hole may have either constructive or destructive interference or both. The total contribution at the focus oscillates with the ratio of d/w. The largest focal amplitude corresponding the first-order diffraction from a single hole is achieved when $d = 1.53w$. Using this rule, we generated a fractal holey metal microlens structure, as shown in **Figure 1**a. Considering our fabrication capablility, we set the hole diameter as small as 60 nm, which corresponds to the outmost zone width of 39 nm. Figure 1b shows the scanning electron microscopy (SEM) image of the fabricated fractal holey-metal microlens structure, which consist of five circular zones of isolated, randomly distributed circular holes. The sizes of innermost and outmost holes are about 1714 and 60 nm in diameter, respectively. The whole pattern area is ~12.25 μm in diameter. Note that some adjacent nanoholes may be connected instead of isolated from the magnified SEM images (see Figure S2a–2d), especially for the outmost zone. However, this shows negligible effect on the focusing performance, which is verified by both experimental and simulation results in the following.

Figure 2a and b represent the simulated and measured field intensity in a cross section through the center of the fractal holey metal microlens (along the x-direction). Both the simulation and the measurement demonstrate clear focusing of the optical wave. Note that the simulation image is generated using the designed parameters in Figure 1a rather than the actual ones measured in the SEM image. Excellent agreement between experiment and simulation is observed, which indicates the robustness in design and the fault tolerance in fabrication for focusing. A more detailed quantitative comparison between the experimental and simulation results is shown in Figure 2c, which is the cross section of the intensity distributions through the focus spots of Figure 2a and b in z-direction. From Figure 2c, we can see that the simulated field intensity distributions are in a reasonable agreement with the experimentally achieved ones. A slight deviation is observed when the light propagates further away from the lens. This is understandable since the confocal microscopy collects light only from a finite diffraction-limited volume. Accumulated scanning errors of the piezo nanopositioning stage may be caused to affect the collected light intensity.

The designed fractal holey-metal microlens shows interesting focusing properties: the light firstly focuses near the exit plane of microlens, bifurcates with the propagation, and then focuses again at a further propagation distance. We therefore checked the cross section of the intensity distributions at these three regimes in x-direction. **Figure 3** and **Figure 4** show the intensity distributions at two focal points of $z = 1.55$ μm and $z = 11.22$ μm. Both 2D and 3D intensity distributions show strong focusing properties. At focal point of $z = 1.55$ μm, the full width at half-maximum (FWHM) is 640 nm and the depth of focus (DOF, defined as the distance between the two halves of the maximum intensity) is 1.28 μm; while at focal point of $z = 11.22$ μm, the FWHM and the DOF are 662 nm and 2.86 μm, respectively. The FWHM of the focal points in our fractal holey-metal microlens is comparable to other reported metallic microlenses based on the same diffractive effect.[30–32] However, there is still

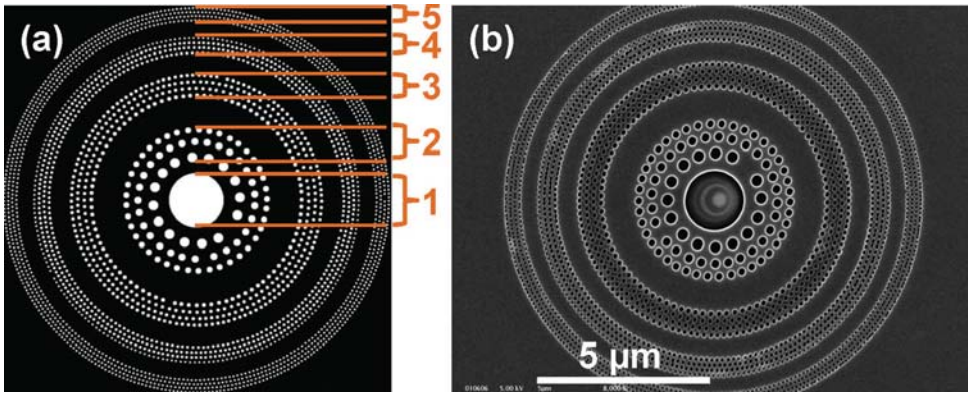

Figure 1. Computer-generated (a) and lithographically fabricated (b) fractal holey metal microlens structures that consist of five zones as shown in (a).

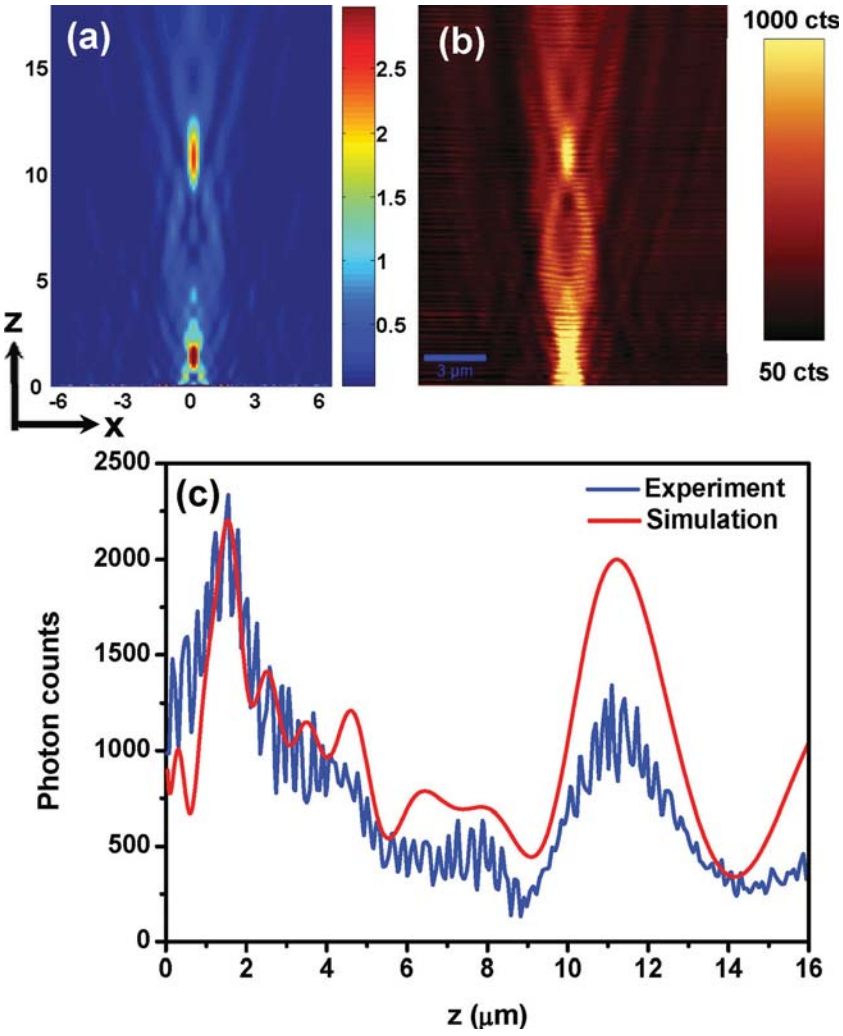

Figure 2. Simulated (a) and measured (b) focusing patterns of the field intensity in the *x*–*z* cross section (sharing the same *z*-axis) through the center of the fractal holey-metal microlens. (c) Simulated (red curve) and measured (blue curve) photon counts (proportional to intensity) in cross section of the focus along the *z*-direction. Total field scattered field (TFSF) source and collimated laser beam with the wavelength of 488 nm are used for simulation and measurement respectively.

much room to improve the FWHM. For example, the FWHM could be greatly improved by blocking the central zones.[35] For plasmonic or metallic microlenses, the optical efficiency is an extremely important concern since it is significantly low due to the high absorption loss, especially for very thick (>100 nm) metal films, which may hinder their practical applications. Therefore, we chose a 50 nm-thick gold film in our experiments, which has relatively low absorption and high transparency. However, for microlenses, it is very challenging to directly measure their focusing efficiency. From our confocal measurements, the intensity ratios of the foci to the incident laser were evaluated to be about 11 (z = 1.55 μm) and 5.5 (z = 11.22 μm), respectively, which should be much higher than other reported metallic lenses based on very thick metal films (>100 nm).[27–32] These achieved intensity ratios indicate a quite high focusing efficiency for our fractal holey-metal microlenses. In addition, the side lobe level (SLL, defined as $10\log_{10}\left(I_{side\_lobe}/I_{principle}\right)$) of about −4.9 dB was achieved at the focal point of z = 11.22 μm in our fractal holey-metal microlens, which was comparable to the ones (~−4dB) in other diffraction-based plasmonic lenses.[36,37] We also did not observe the odd higher-order foci clearly. This is a big advantage that both the side lobes and the high-order diffractions (i.e., odd higher-order foci) are suppressed over conventional FZPs, in which a ring shaped secondary maxima (i.e., side lobes or halo effect) and odd higher-order foci (f/3, f/5, ...) are produced simultaneously in addition to the principal focus. The halo effect associated with conventional FZPs will greatly increase the SLL and blur the imaging qualities. Meanwhile, the odd higher-order foci dissipate the optical energy undesirably along the optical axis. **Figure 5** shows the intensity distributions at z = 8 μm, which is in between those two focusing regimes. It is interesting that a light well (i.e., annular ring-shape light intensity distributions) is formed, which is in good agreement with the FDTD simulations. Such a light well is potentially useful for trapping and sorting of cells and particles.[38]

The improvements on SLL and higher order foci arise from fractal nature with the smoothing effect that the nanoholes produce on each ring. In our fractal holey metal microlens, the normal incidence of light on the microlens surface will induce excitation of surface plasmons in the nanohole array: plasmon oscillations that are in-phase among same-size-nanoholes on the input surface (quartz–gold interface) still remain in-phase on the output surface (gold–air interface) after transmission. In such a process, surface plasmons play a facilitating role on enhancing the light transmission and ultimately improving the focusing efficiency of our fractal holey metal microlens. However, the focusing performance will be still mainly governed by the diffractive effect of structures. Since a very thin gold film is used in our experiments, the thickness of the gold film induced negligible phase retardation among the nanoholes in the zones from No. 2 to No. 5 except the innermost hole. Therefore, we can consider every nanohole as a secondary light source. In such a case, when an optical system with two-dimensional pupil function $p(r, \phi)$ is illuminated by a plane wave with a wavelength of λ, the irradiance along the optical axis z can be expressed in canonical polar coordinates as expressed below:

$$I(z)=\left(\frac{2\pi}{\lambda_0 z}\right)^2\left|\int_0^a\int_0^{2\pi} p(r,\phi)\exp\left(i\frac{\pi}{\lambda_0 z}r^2\right)r\,dr\,d\phi\right|^2. \quad (1)$$

The axial irradiance in Equation (1) can be conveniently expressed in terms of a single radial integral by performing first the azimuthal average of the pupil function $p(r, \phi)$:

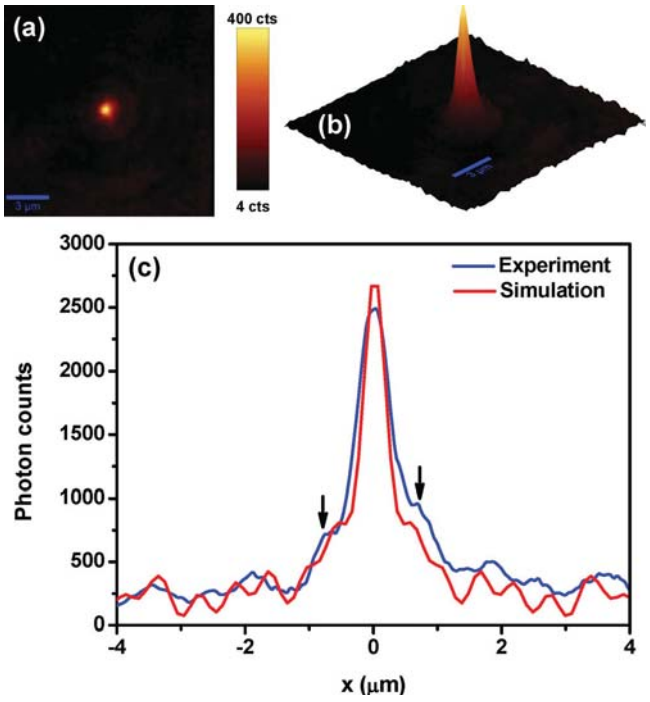

Figure 3. 2D (a) and 3D (b) intensity distributions at z = 1.55 μm. (c) Finite-difference time-domain (FDTD) simulated (red curve) and photon scanning tunnelling microscope (PSTM) measured (blue curve) intensity distributions in cross section of the quasi-near-field focus along the x-direction. Side lobes are marked by arrows.

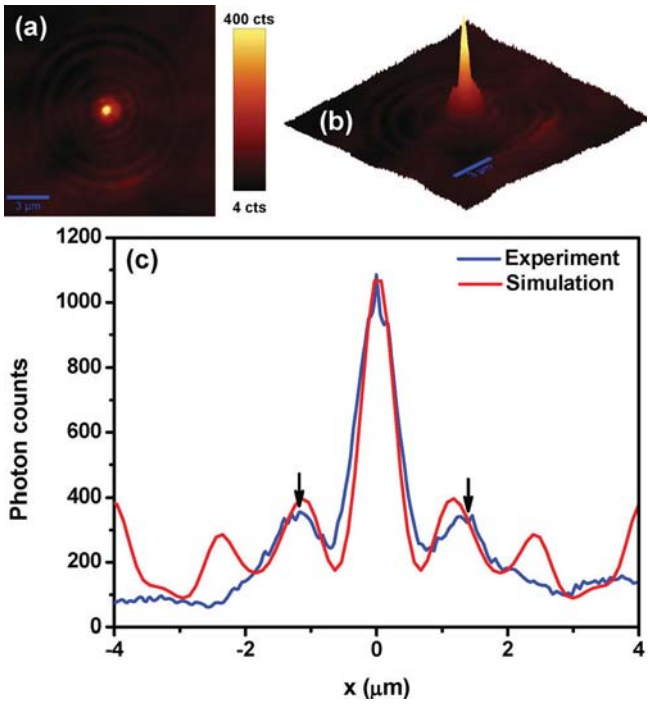

Figure 4. 2D (a) and 3D (b) intensity distributions at z = 11.22 μm. (c) FDTD simulated (red curve) and PSTM measured (blue curve) intensity distributions in cross section of the far-field focus along the x-direction. Side lobes are marked by arrows.

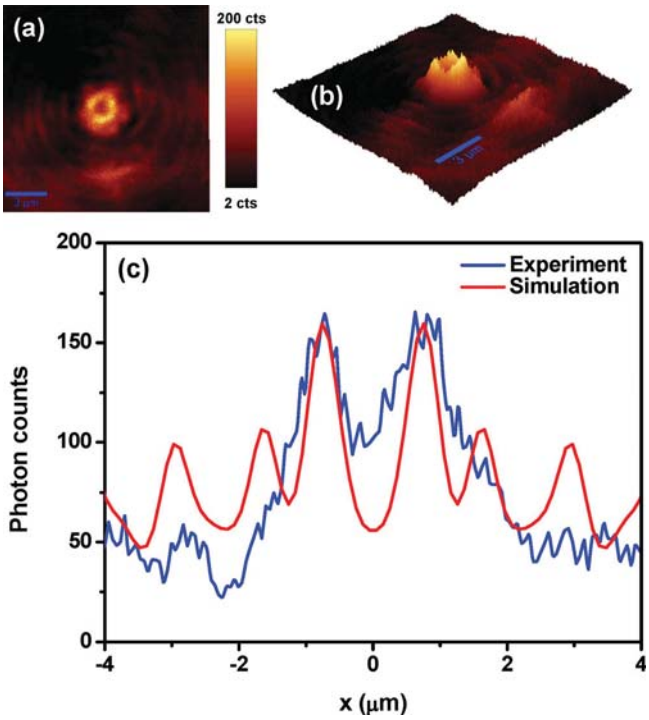

Figure 5. 2D (a) and 3D (b) intensity distributions at z = 8 μm. (c) FDTD simulated (red curve) and PSTM measured (blue curve) intensity distributions in cross section along the x-direction.

$$p_0(r_0) = \frac{1}{2\pi}\int_0^{2\pi} p(r_0,\phi)\,d\phi. \tag{2}$$

Then Equation (1) can be rewritten as

$$I(z) = \left(\frac{2\pi}{\lambda_0 z}\right)^2 \left|\int_0^a p_0(r_0)\exp\left(i\frac{\pi}{\lambda_0 z}r_0^2\right) r_0\,dr_0\right|^2. \tag{3}$$

From Equation (3), we can see that the azimuthal average of the pupil accounts ultimately for the behavior of the axial irradiance, instead of the pupil itself. In our fractal design, we render all the nanoholes in each zone to have constructive contributions to the principal focus but destructive contributions (tends to zero) to the higher-order foci. Our calculations based on Equation (3) show that the intensity of the higher-order foci decreases exponentially with the increase of the diffraction orders. For example, the intensities of third-order and fifth-order foci are at least three and seven times less than that of the principle focus. On the other hand, from Figure 1, the size of the nanoholes on zones from No. 2 to No. 5 gradually decreases from inside to outside. The gradual size changes create a smooth filtering effect and hence effectively suppress the side lobes around the principle focus.[5] Therefore, both the side lobes and the odd higher orders are highly suppressed due to the combined effects by the fractal nature and the smooth filtering effect.

To reveal the focusing nature of our designed fractal holey-metal microlens, we further decomposed its structure into two parts: the single innermost hole (Figure S3a) and the outer zones from No. 2 to No. 5 (Figure S3b). Figure S3c and S3d show the simulated field intensity distribution of the

decomposed structures in Figure S3a and S3b. From Figure S3c and S3d, it is clear that the quasi-near-field focusing arises primarily from the diffraction of the innermost hole; while the far-field focusing is mainly attributed to the constructive interference of optical waves emerging from the nanoholes inside the outer zones from No. 2 to No. 5. It is worth mentioning that FDTD simulations show slightly decreased DOF of 2.18 μm in Figure S3d compared to DOF of 2.39 μm in Figure 2a, which may be attributed to the cancellation of the constructive interference between the emerging light from the innermost hole and the outer zones.

To validate our simulations, we fabricated exactly the same structure as showed in Figure S3b by only removing the innermost hole. **Figure 6**a shows the SEM image of the fractal holey-metal microlens without the innermost hole. The confocal measurement and cross-section analysis at the focal plane are shown in Figure 6b–e. We can see that the fractal holey-metal microlens without the innermost hole has only one far-field focal point at ~11.2 μm. More importantly, a significantly improved SLL of −10 dB (see Figure 6e) is experimentally achieved compared to the one with the innermost hole (see Figure 4c). The central block zone can efficiently eliminate the background from the diffraction other than the first order and further suppress the side lobes. Simpson and Michette have proven that blocking the central zones of a zone plate can efficiently remove the effect of non-diffracted radiation (i.e. the 0th-order radiation or background).[35] By blocking the central zone, the focus of our fractal holey-metal microlens is formed in the shadow of the obstruction, hence producing a high-contrast focusing. In addition, due to the central blocked zone, the focal depth is also increased by a factor of $1/(1-a^2)$, where a^2 is the fraction of the area blocked. Compared to the one with the innermost hole, the addition of the central blocked zone, i.e., a 50-nm thin gold layer, causes significant absorption (~89% for the wavelength of 488 nm), which hence causes the absorption-induced apodization of the illumination. Guo and Barton have demonstrated that for a centrally opaque zone plate, adequately lowering the illumination can efficiently reduce the SLL.[39] Therefore, in our fractal holey-metal microlens, the side lobes are significantly suppressed due to the absorption-induced apodization of the illumination. The analysis for the experimental results shows that the focal points of the microlens before and after the removal of the innermost hole have almost the same FWHM as expected. It is also worth mentioning that since our design supports axial symmetry both globally (in the rings of holes) and locally (for each circular nanohole), the device can focus normally incident, linearly polarized light with any polarization angle (i.e. linear-polarization insensitive, see Figure S4).

3. Conclusion

We have demonstrated a fractal holey-metal microlens based on finite-areas of two-dimensional arrays of circular nanoholes. Due to the fractal design with nanohole-enhabled smoothing effect, both the side lobes (i.e. the halo effect) and the odd higher orders associated with the conventional Fresnel zone plates can be greatly suppressed in our fractal holey metal microlens. In addition, a relatively high lens efficiency has been achieved. The ultra-thin, planar and compact design allows

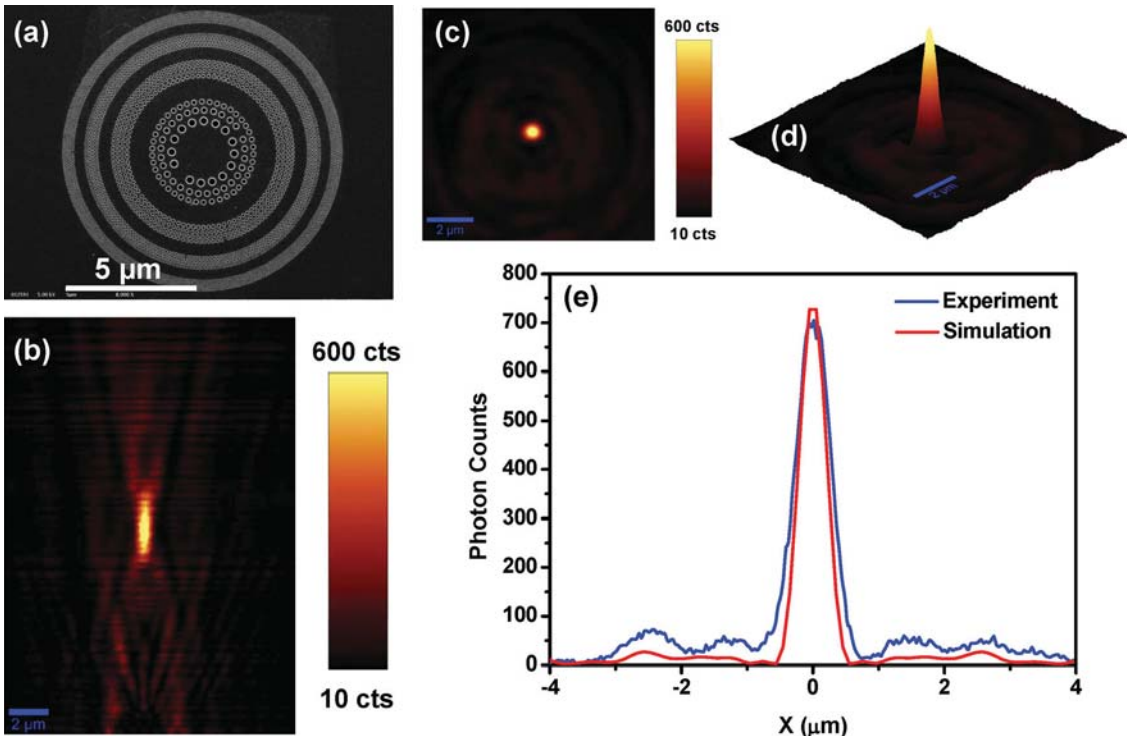

Figure 6. (a) SEM image of the fractal holey metal microlens without the innermost hole. PSTM measured intensity distributions in cross sections of the focus along the *z*-direction (b) and *x*-direction (c and d). The *z*-span in Figure (b) is from 0 (bottom) to 20 μm (top). (e) Simulated and measured intensity distributions in cross section along the *x*-direction. Collimated laser beam with the wavelength of 488 nm was used for measurement.

for large-scale fabrication of microlens arrays and convenient integration with other optical systems. The excellent focusing performance and controllable focal length in micronmeter scale enable our fractal holey metal microlenses promising for bio-imaging, optical trapping, and integrated optics.

4. Experimental Section

Fractal Holey Metal Microlens Fabrication: A 50-nm thick Au film was first deposited with an adhesion layer of 2-nm chromium onto quartz substrates with a refractive index of 1.46 by electron beam evaporation (Denton Vacuum Explorer) at room temperature. The pattern of the fractal holey-metal microlens was written by electron-beam lithography (ELS-7000, Elionix). ZEP-520A resist (1:1 ratio mixing with anisole) was spin-coated at 5000 rpm followed by soft-baking at 180 °C for 2 min on a hotplate. The exposure conditions were configured with an exposure dosage of 520 μC/cm^2 and beam current of 50 pA. Subject to a dry etching process, the fractal holey-metal microlens was formed on the Au layer after stripping the residual layer.

Confocal Measurements: The performance of the fractal holey metal microlens was evaluated using the confocal scanning function of a photon scanning tunnelling microscope (PSTM, *alpha*-300S, WITec). The sample was illuminated with a collimated, polarized laser beam from the substrate side. The laser beam has a diameter of ~10 mm. The sample was mounted on a closed loop XYZ piezo nanopositioning stage such that the planar microlens was situated in the *x*–*y* plane with its optical axis orientated along the *z* direction. The transmitted beam through the lens was collected by an objective (Olympus, 100×, 0.9 NA), focused down to a 100 μm multimode fiber that serves as a pinhole in the system, and eventually detected by a photomultiplier tube (PMT). The three-dimensional (3D) spatial intensity profile of the transmitted beam was obtained by taking a sequence of 2D intensity profiles (on the *x*-*y* plane) at different *z* positions along the propagation direction. The scan in the *x*-*y* plane was 15 × 15 μm^2 with total 256 × 256 pixels (i.e., ~60 nm/pixel resolution), and the step size along *z* direction was 200 nm. The signal-to-noise ratio of the system at the exit interface of the structure was 100:1.

Optical Simulations: To model the focusing performance of the fractal holey-metal microlens, we carried out the finite-difference time-domain (FDTD) calculations using a commercial software (Lumerical). The designed structure was directly imported into the software. The whole structure was simulated with perfectly matched layer (PML) boundary condition in the *x*-, *y*-, and *z*-direction. The mesh size of the simulation space was 10 nm (Δx) × 10 nm (Δy) × 11 nm (Δz). We injected a total field scattered field (TFSF) source with polarization direction along the *x*-axis from the bottom of the quartz substrate. The dispersion of gold was based on the Johnson and Christy model[40] in the material library of the software.

Supporting Information

Supporting Information is available from the Wiley Online Library or from the author.

Acknowledgements

This work was financially supported by Agency for Science, Technology and Research (A*STAR), under the grant No. 12302FG012, 0921540098, and 0921540099.

Received: October 31, 2013
Revised: February 1, 2014
Published online: March 20, 2014

[1] N. Bokor, N. Davidson, *Rev. Sci. Instrum.* **2005**, *76*, 111101.
[2] F. M. Dickey, *Opt. Photonics News* **2003**, *14*, 30.
[3] D. G. Grier, *Nature* **2003**, *424*, 810.
[4] Y. X. Wang, W. B. Yun, C. Jacobsen, *Nature* **2003**, *424*, 50.
[5] L. Kipp, M. Skibowski, R. L. Johnson, R. Berndt, R. Adelung, S. Harm, R. Seemann, *Nature* **2001**, *414*, 184.
[6] Q. Cao, J. Jahns, *J. Opt. Soc. Am. A* **2002**, *19*, 2387.
[7] Q. Cao, J. Jahns, *J. Opt. Soc. Am. A* **2003**, *20*, 1005.
[8] G. Andersen, *Opt. Lett.* **2005**, *30*, 2976.
[9] R. Menon, D. Gil, G. Barbastathis, H. Smith, *J. Opt. Soc. Am. A* **2005**, *22*, 342.
[10] G. Andersen, D. Tullson, *Appl. Opt.* **2007**, *46*, 3706.
[11] J. Jia, J. Jiang, C. Xie, M. Liu, *Opt. Commun.* **2008**, *281*, 4536.
[12] B. B. Mandelbrot, *The Fractal Geometry of Nature*, W. H. Freeman, San Francisco **1982**.
[13] G. Saavedra, W. D. Furlan, J. A. Monsoriu, *Opt. Lett.* **2003**, *28*, 971.
[14] W. D. Furlan, G. Saavedra, J. A. Monsoriu, *Opt. Lett.* **2007**, *32*, 2109.
[15] W. L. Barnes, A. Dereux, T. W. Ebbesen, *Nature* **2003**, *424*, 824.
[16] E. Ozbay, *Science* **2006**, *311*, 189.
[17] J. B. Pendry, L. Martin-Moreno, F. J. Garcia-Vidal, *Science* **2004**, *305*, 847.
[18] T. W. Ebbesen, H. J. Lezec, H. F. Ghaemi, T. Thio, P. A. Wolff, *Nature* **1998**, *391*, 667.
[19] F. J. Garcia-Vidal, H. J. Lezec, T. W. Ebbesen, L. Martin-Moreno, *Phys. Rev. Lett.* **2003**, *90*, 213901.
[20] H. Liu, P. Lalanne, *Nature* **2008**, *452*, 728.
[21] S. I. Bozhevolnyi, V. S. Volkov, E. Devaux, J.-Y. Laluet, T. W. Ebbesen, *Nature* **2006**, *440*, 508.
[22] S. Lal, S. Link, N. J. Halas, *Nat. Photon.* **2007**, *1*, 641.
[23] J. A. Dionne, H. J. Lezec, H. A. Atwater, *Nano Lett.* **2006**, *6*, 1928.
[24] M. T. Hill, Y.-S. Oei, B. Smalbrugge, Y. Zhu, T. de Vries, P. J. van Veldhoven, F. W. M. van Otten, T. J. Eijkemans, J. P. Turkiewicz, H. d. Waardt, E. J. Geluk, S.-H. Kwon, Y.-H. Lee, R. Notzel, M. K. Smit, *Nat. Photon.* **2007**, *1*, 589.
[25] R. F. Oulton, V. J. Sorger, T. Zentgraf, R.-M. Ma, C. Gladden, L. Dai, G. Bartal, X. Zhang, *Nature* **2009**, *461*, 629.
[26] M. A. Noginov, G. Zhu, A. M. Belgrave, R. Bakker, V. M. Shalaev, E. E. Narimanov, S. Stout, E. Herz, T. Suteewong, U. Wiesner, *Nature* **2009**, *460*, 1110.
[27] Z. Liu, S. Durant, H. Lee, Y. Pikus, N. Fang, Y. Xiong, C. Sun, X. Zhang, *Nano Lett.* **2007**, *7*, 403.
[28] F. M. Huang, T. S. Kao, V. A. Fedotov, Y. Chen, N. I. Zheludev, *Nano Lett.* **2008**, *8*, 2469.
[29] G. M. Lerman, A. Yanai, U. Levy, *Nano Lett.* **2009**, *9*, 2139.
[30] L. Verslegers, P. B. Catrysse, Z. Yu, J. S. White, E. S. Barnard, M. L. Brongersma, S. Fan, *Nano Lett.* **2009**, *9*, 235.
[31] L. Lin, X. M. Goh, L. P. McGuinness, A. Roberts, *Nano Lett.* **2010**, *10*, 1936.
[32] S. Ishii, V. M. Shalaev, A. V. Kildishev, *Nano Lett.* **2013**, *13*, 159.
[33] E. T. F. Rogers, J. Lindberg, T. Roy, S. Savo, J. E. Chad, M. R. Dennis, N. I. Zheludev, *Nat. Mater.* **2012**, *11*, 432.
[34] H. T. Dai, J. H. Liu, X. C. Sun, D. J. Yin, *Opt. Commun.* **2008**, *281*, 5515.
[35] M. J. Simpson, A. G. Michette, *Optica Acta* **1984**, *31*, 403.
[36] S. Ishii, V. P. Drachev, A. V. Kildishev, *Opt. Commun.* **2012**, *285*, 3368.
[37] F. Aieta, P. Genevet, M. A. Kats, N. Yu, R. Blanchard, Z. Gaburro, F. Capasso, *Nano Lett.* **2012**, *12*, 4932.
[38] B. Shao, L. Z. Shi, J. M. Nascimento, E. L. Botvinick, M. Ozkan, M. W. Berns, S. C. Esener, *Biomed. Microdevices* **2007**, *9*, 361.
[39] Y. J. Guo, S. K. Barton, *IEEE Int. Symp. Antennas Propagation Digest* **1992**, 2175.
[40] P. B. Johnson, R. W. Christy, *Phys. Rev. B* **1972**, *6*, 4370.